Development/Plasticity/Repair

Control of Cellular Pattern Formation in the Vertebrate Inner Retina by Homotypic Regulation of Cell-Fate Decisions

Melinda J. Tyler,[1,2] Laurel H. Carney,[3] and David A. Cameron[1]

[1]Department of Neuroscience and Physiology and [2]MD/PhD Program, State University of New York Upstate Medical University, Syracuse, New York 13210, and [3]Institute for Sensory Research, Department of Biomedical and Chemical Engineering and Department of Electrical Engineering and Computer Science, Syracuse University, Syracuse, New York 13244-1240

The vertebrate retina is composed of cellular arrays that are nonrandom across two-dimensional space. The determinants of these nonrandom two-dimensional cellular patterns in the inner nuclear layer of the retina were investigated using empirical and computational modeling techniques. In normal and experimental models of goldfish retinal growth, the patterns of tyrosine hydroxylase- and serotonin-positive cells indicated that neither cell death nor lateral migration of differentiated cells were dominant mechanisms of cellular pattern formation. A computational model of cellular pattern formation that used a signaling mechanism arising from differentiated cells that inhibited homotypic cell-fate decisions generated accurate simulations of the empirically observed patterns in normal retina. This model also predicted the principal atypical cellular pattern characteristic, a transient cell-type-specific hyperplasia, which was empirically observed in the growing retina subsequent to selective ablation of differentiated retinal cells, either tyrosine hydroxylase positive or serotonin positive. The results support the hypothesis that inhibitory spatiotemporal regulation of homotypic cell-fate decisions is a dominant mechanistic determinant of nonrandom cellular patterns in the vertebrate retina.

Key words: **retina; development; growth; patterning; modeling; computational**

Introduction

At the cellular level, the vertebrate retina is characterized by a high degree of spatial order across its tangential plane, and this structural organization is likely to be a key contributor to the functional characteristics of the retina. Although these nonrandom two-dimensional (2D) cellular patterns are common across the vertebrate subphylum, the mechanisms that drive their formation during retinal growth are not completely understood. Empirical and computational investigations of cellular pattern formation in the vertebrate retina have, however, generated specific theories regarding the mechanisms that position cells within two-dimensional space. Three of these hypothesized mechanisms are the spatiotemporal control of cell-fate decisions (Eglen and Willshaw, 2002; Frankfort and Mardon, 2002; Cameron and Carney, 2004), lateral migration of differentiated cells (Hendrickson, 1994; Reese et al., 1995, 1999; Galli-Resta et al., 1997; Eglen et al., 2000; Galli-Resta, 2000), and spatial patterns of apoptosis (Jeyarasasingam et al., 1998; Cusato et al., 2001; Eglen and Willshaw, 2002; Raven et al., 2003). Each of these mechanisms may function coincidentally or at disparate times during development (for review, see Cook and Chalupa, 2000).

In the current investigation, a combination of empirical and computational modeling techniques was used to explicitly evaluate and differentiate these three hypothesized mechanisms. For the empirical analyses, longitudinal growth assessment, cellular death determination, selective cellular ablation, and quantitative spatial pattern analyses were applied to the growing retina of adult goldfish. In the computational analyses, a model of cellular pattern formation in the vertebrate retina, based on a physiologically realistic signaling strategy (Cameron and Carney, 2004), was used to generate predictions of cellular pattern formation in normal and cell-ablated retinas. For two independent "cell types" of the inner nuclear layer [tyrosine hydroxylase positive (TH^+) and serotonin immunopositive ($5\text{-}HT^+$)], the empirical investigations revealed no evidence that either cell death or lateral migration of differentiated cells was significantly contributing mechanisms to cellular pattern formation during retinal growth. Application of the computational model and its direct comparison with the empirically derived data indicated that cellular pattern formation in this system could be dominated by signals arising from differentiated neurons that inhibit homotypic cell-fate decisions at the neurogenic epithelium of the retina. Because the two-dimensional patterns of the analyzed cell types are independent, the coincident operation of multiple independent cell type-specific controlling mechanisms was inferred. Finally, the results motivated the development of a model of cellular pattern formation in the growing retina in which cell-fate decisions at the neurogenic epithelium are hypothesized to be controlled, at least in part, by neurotransmitter signaling.

Received Feb. 12, 2005; revised March 25, 2005; accepted March 26, 2005.

This work was supported by National Science Foundation Grant 0351250 (D.A.C.). We thank Michelle Mader, Yumiko Umino, and Patrick Yurco for helpful discussions and comments on this manuscript.

Correspondence should be addressed to David A. Cameron, Department of Neuroscience and Physiology, State University of New York Upstate Medical University, 750 East Adams Street, Syracuse, NY 13210. E-mail: camerond@upstate.edu.

DOI:10.1523/JNEUROSCI.0588-05.2005

 0270-6474/05/254565-12$15.00/0

Materials and Methods

Model system and intraocular drug delivery. Light-adapted goldfish (*Carassius auratus*) of 4.1–6.3 cm standard body length were used for all experiments, which were approved by the Committee for the Humane Use of Animals at the State University of New York Upstate Medical University. Fish received one-time 1 μl intraocular injections in their left eyes of a 0.9% saline solution containing 5 mM 5-bromo-2′-deoxyuridine (BrdU) to label proliferative cells at the circumferential germinal zone (CGZ) or their terminally differentiated progeny (Cameron, 1995). The same solution was injected into the right eyes, supplemented with a neurotoxin that targeted either tyrosine hydroxylase-immunopositive cells [6-hydroxydopamine (6-OHDA)] (Sigma, St. Louis, MO) or serotonin-immunopositive cells [5,7-dihydroxytryptamine (5,7-DHT)] (Sigma). The total amount of 6-OHDA and 5,7-DHT delivered to the eyes was 5 and 15 μg, respectively. Drug selection and injection procedure was based on that described previously by Hitchcock and Vanderyt (1994) and Negishi et al. (1982). After injection, fish were returned to their tanks for times ranging from 1 d to 9 months.

Immunohistochemistry and cell death analysis. The methodology for selectively labeling and visualizing cells in retinal whole mounts or cryosections using indirect fluorescence immunohistochemical techniques was based on that described previously (Cameron and Carney, 2000). Briefly, for whole-mount analysis, light-adapted eyes were fixed (4% paraformaldehyde, 0.25% picric acid, and 0.1 M PO_4 buffer, pH 7.2), and the retinas (with pigmented epithelium attached) were flattened. Retinal whole mounts were then exposed to 5% normal serum (in PBS and 0.3% Triton X-100), followed by a 1% solution of one of two primary antibodies: anti-TH (catalog #MAB318; Chemicon, Temecula, CA) or anti-5-HT (catalog #MAB352; Chemicon). Primary antibody labeling was visualized via fluorophore-conjugated secondary antibody (TH^+ cells) or a combined secondary and tertiary antibody ($5\text{-}HT^+$ cells). When a tertiary antibody was required for visualization, the conjugated fluorophore was matched to that of the secondary antibody, typically cyanine 2 (Cy2) (Jackson ImmunoResearch, West Grove, PA). $BrdU^+$ cells were visualized as described previously (Cameron, 1995; Cameron and Easter, 1995), using either a Cy3- or tetramethylrhodamine isothiocyanate-conjugated secondary antibody (Jackson ImmunoResearch); actively proliferating cells were detected with an antibody against proliferating cell nuclear antigen (PCNA) (catalog #M-0879; Dako, Glostrup, Denmark). The terminal deoxynucleotidyl transferase-mediated biotinylated UTP nick end labeling (TUNEL) method was used to label retinal cells exhibiting evidence of apoptotic cell death 48 h after neurotoxin administration (ApopTag kit; Serologicals, Norcross, GA). The protocol of the TUNEL kit was modified to detect TUNEL-positive cells with a fluorescence reporter (Yurco and Cameron, 2005).

In the current report, the phrase cell type, and its variants, is used solely to indicate detected, labeled, or model-derived cells that share a particular immunohistochemical profile (Cameron and Carney, 2000, 2004).

Quantitative analysis of cellular patterns. Reacted retinal whole mounts were examined with standard epifluorescence light microscopy (Axioskop; Zeiss, Thornwood, NY), and digital images were collected with an associated camera and image analysis system (MetaMorph; Universal Imaging, Teaneck, NJ). For a given retinal field of ~60,000 μm^2, a two-dimensional (x, y) coordinate list of positively labeled cells was established, with the center of the optic nerve defined as the coordinate origin. For estimates of cellular density relative to the band of $BrdU^+$ cells (see Results), virtual strips of 20 μm thickness were defined parallel to and starting from the innermost edge of the $BrdU^+$ band. Labeled cells were counted within each strip, and the total cell count was divided by the strip area to derive an estimate of cellular density. Statistical comparison of cellular density between control and experimental (i.e., neurotoxin exposure) conditions was achieved with an independent Student's t test.

For both empirical- and model-derived (see below) data, the two-dimensional patterns of labeled cells were analyzed quantitatively with three previously described spatial-analysis techniques: nearest-neighbor distance (NND) (Cook, 1996), density recovery profile (DRP) (Rodieck, 1991), and quadrat analysis (Grieg-Smith, 1964). The details, statistical utility, and application of these techniques, including their application to empirical- and model-derived cellular patterns in the retina, have been described previously (Cameron and Carney, 2000, 2004; Stenkamp et al., 2001). Briefly, NND analysis provides a measure of local pattern regularity or nonregularity. From the NND distribution of a sample, a value, termed the conformity ratio, is derived (mean ± SD of the NND distribution), from which a statistical assessment of pattern regularity is achieved (Cook, 1996). From the DRP analysis, a metric is derived, termed the effective radius, which provides evidence for the presence or absence of anticlustering phenomena among the cells within the sample; the estimated density of the analyzed cells is also "recovered" (Rodieck, 1991). Quadrat analysis derives a statistic, termed a dispersion "index," which characterizes the long-range patterning attribute of a sample as regular, aggregated (clumpy), or neither regular nor aggregated (e.g., random). NND and DRP analyses were performed in either autocorrelation (homotypic) or cross-correlation (heterotypic) modes.

Computational modeling. A computational model of cellular pattern formation in the growing retina, the details of which have been described previously (Cameron and Carney, 2004), was used to formulate and test hypotheses of the mechanisms of retinal cell-pattern formation. Briefly, the model used an exponentially decaying signal, arising from each member of an *in vivo*, empirically derived "seed" of differentiated retinal cells of a particular type, which inhibited the production of homotypic cells at the CGZ (i.e., the proliferative neurogenic epithelium of the retina). For each simulation, a random set of locations was used for the precursor cells in the CGZ. Application of the model involved the determination of the space constant (λ) of the inhibitory signal that resulted in a model-derived pattern of cells with an NND distribution that was not significantly different from that of the seed (Student's t test). After determina-

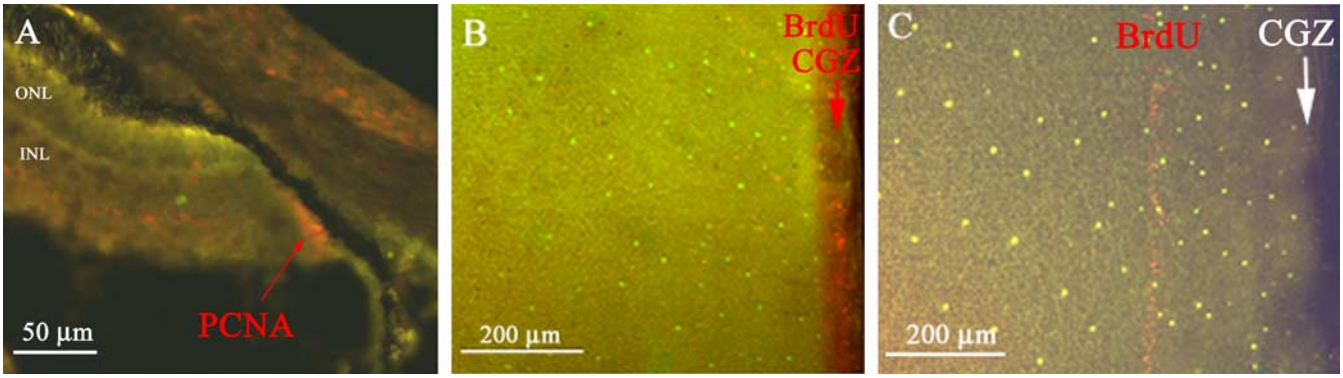

Figure 1. Confirmation of retinal growth from the CGZ. ***A***, $PCNA^+$ cells (red cells; arrow) are located at the CGZ, as expected for a proliferative neuroepithelium at the retinal margin. ONL, Outer nuclear layer; INL, inner nuclear layer. ***B***, Whole-mounted retina that was exposed to BrdU for 2 h immediately before tissue processing (see Materials and Methods). $BrdU^+$ cells are located primarily at the CGZ (red cells). TH^+ cells are also evident (green cells). ***C***, Whole-mounted retina that was exposed to a single dose of BrdU 9 months before tissue processing. Note the persistence of a $BrdU^+$ terminally differentiated band of cells displaced centrally from the retinal margin, consistent with substantial retinal growth after BrdU exposure. TH^+ cells are evident as in ***B***.

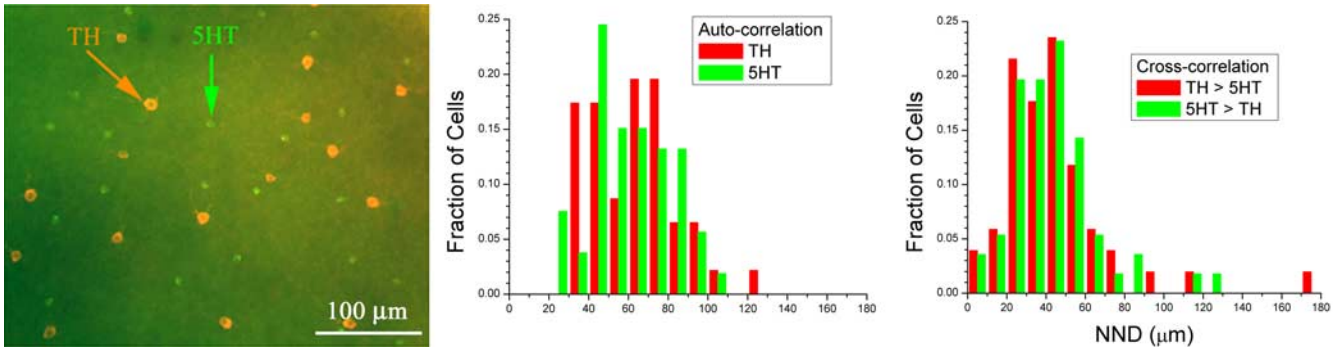

Figure 2. NND analysis of empirically observed cellular patterns. Top, TH$^+$ (red) and 5-HT$^+$ (green) cells in whole-mounted retina. Middle, Autocorrelational NND analyses for a representative whole-mount image of a retina double labeled for TH$^+$ and 5-HT$^+$ cells. Conformity ratio analysis indicated that all patterns were nonrandom and characterized by local homotypic zones of exclusion (Cook, 1996) (see Results) (Table 1). Bottom, Cross-correlational NND analyses for the same pattern of cells. Note the leftward shift of the distributions relative to the corresponding autocorrelational distributions, indicating an apparent lack of local heterotypic zones of exclusion. Conformity ratio analysis indicated that the heterotypic cell patterns were independent (see Results), similar to analyses of these cell types in zebrafish retina (Cameron and Carney, 2000, 2004).

Table 1. Statistical analyses for *in vivo* patterns of TH$^+$ and 5-HT$^+$ cells in control retinas double labeled for both cell types

Cell type	aNND (μm)	Quadrat	aR_{eff} (μm)	CNND (μm)	cR_{eff} (μm)
TH	63.9 ± 20.1 (35)	Regular	54.1	42.0 ± 26.4 (59)	18.5
5-HT	62.0 ± 20.0 (45)	Regular	46.6	41.6 ± 21.8 (64)	18.5
TH	63.0 ± 16.4 (42)	Regular	45.2	42.6 ± 22.4 (63)	6.1
5-HT	51.0 ± 20.2 (43)	Regular/random	45.5	39.9 ± 22.4 (67)	6.1
TH	84.2 ± 15.0 (26)	Regular	68.2	34.2 ± 16.1 (44)	0
5-HT	61.7 ± 15.1 (49)	Regular	51.6	43.6 ± 20.3 (69)	0

Data are from fish that were not subjected to any experimental manipulations. Data in each row correspond to cellular patterns derived from one representative image. All NND and effective radius values are presented as mean ± SD (number of cells in retinal image). a, Auto-correlation mode; c, cross-correlation mode; R_{eff}, effective radius derived from DRP analysis.

tion of the value for λ, several model-derived patterns ($n \geq 3$ for each seed pattern) were further compared with the seed using DRP and quadrat analyses. For modeling cellular pattern formation subsequent to cell ablation, the seed of differentiated cells was removed (ablated), and the λ value was assigned to that determined for the corresponding control retina. The density of precursor cells in the CGZ was assigned a constant value of 100,000 cells/mm^2, a mean value estimated from toluidine blue labeling of CGZ cells in five radial sections obtained from a control retina. A 50-μm-wide arc of precursor cells was added for each step of the simulation. Locations of precursor cells were uniformly distributed across each newly added arc. Additional details of the model are included in the supplemental material (available at www.jneurosci.org).

Results

Growth and structure of cellular patterns in normal retina

Analyses of PCNA labeling and BrdU incorporation confirmed cell-cycle progression at the CGZ and CGZ-mediated retinal growth. Specifically, PCNA-positive cells were located at the extreme margin of all retinas (Fig. 1*A*), corresponding to the location of the CGZ (Johns, 1977; Easter, 1992; Cameron 1995). BrdU incorporation was also observed in this location (Fig. 1*B*), supporting the interpretation of a proliferative neuroepithelium at the retinal margin. Longitudinal BrdU analysis revealed that, over time, some proliferative cells at the CGZ cease to proliferate; that is, the BrdU label was not diluted away by subsequent passages through the cell cycle. These cells retain the BrdU marker after their terminal mitosis, and they become displaced centrally (but apparently do not migrate; see below) by subsequent cellular addition to the retina from the CGZ (Fig. 1*C*).

The 2D patterns of two inner nuclear layer cell types (TH$^+$ and 5-HT$^+$) were quantitatively analyzed. Both cell types were arrayed in 2D patterns that were nonrandom (Fig. 2). Visual inspection of the patterns of both cell types suggested characteristics of regularity and local anticlustering (Fig. 2, top). Additionally, for both cell types, autocorrelation NND (aNND) analysis revealed pattern characteristics that were significantly different from those expected for random distributions of the same number of cells within the same two-dimensional areas, as reported previously for the same cell types in zebrafish retina (Cameron and Carney, 2004). The aNND distributions for each cell type were normally distributed (Fig. 2, middle), and conformity ratio analysis indicated that the patterns were regular and significantly different from those expected for random patterns ($p < 0.01$; $n = 3$ retinas for each cell type and a mean of 34 and 45 for TH$^+$ and 5-HT$^+$ cells, respectively, per data set). Autocorrelation DRP (aDRP) analysis also indicated that the cellular patterns were nonrandom and characterized by local anticlustering: each soma was surrounded by a 2D zone of exclusion within which the probability of another like-type soma was low, as defined by effective radius values that were substantially greater (fivefold or more) than the soma diameter (Table 1; compare Fig. 2, top). Finally, quadrat analysis revealed that nearly all of the cellular patterns were regular (Table 1); that is, the calculated dispersion index functions were consistently below the regions expected for random or aggregated patterns (Grieg-Smith, 1964). The pattern analyses thus revealed that the 2D patterns of TH$^+$ and 5-HT$^+$ cells in goldfish retina were nonrandom and anticlustered.

For control retinas that had been double labeled for both TH$^+$ and 5-HT$^+$ cells, cross-correlation pattern analyses indicated that the two cell types were arrayed independently across 2D space. The cross-correlational NND (cNND) distributions (Fig. 2, bottom) were all significantly different from the corresponding aNND distributions (Fig. 2, Table 1) (Student's *t* test; $p < 0.02$; $n = 3$ retinas). Independent of the direction of correlation (e.g., TH$^+$ to 5-HT$^+$ or 5-HT$^+$ to TH$^+$), conformity ratio analysis of the cNND pairings revealed that the TH$^+$ and 5-HT$^+$ patterns were arrayed randomly with respect to each other, and thus the location of a given soma provided no predictive information

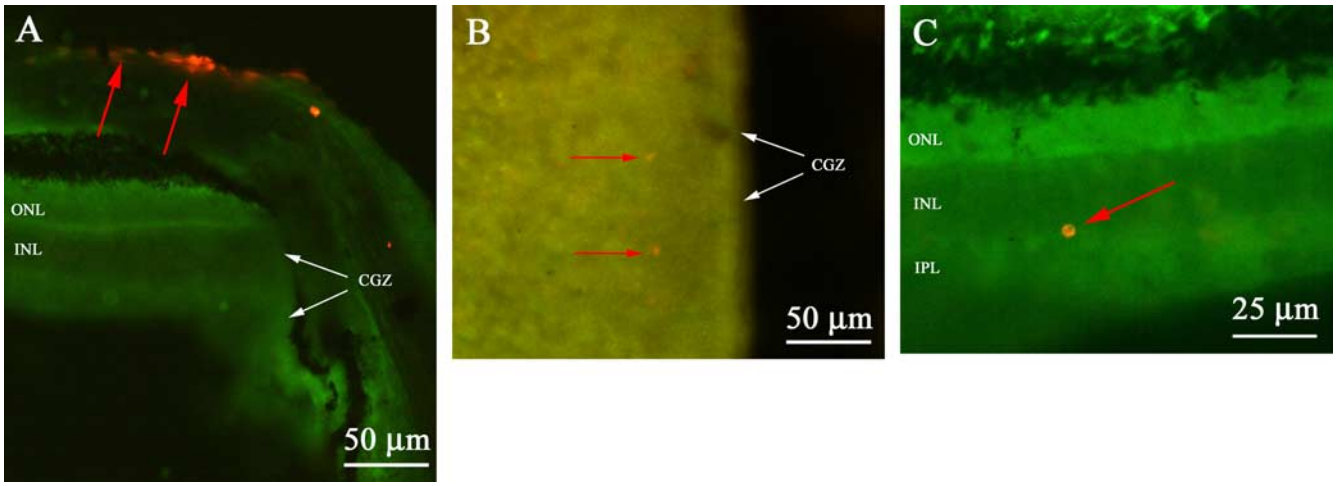

Figure 3. TUNEL-positive cells in goldfish retina. ***A***, In control tissue, the only consistently observed TUNEL-positive cells were located outside the neural retina (red arrows). No TUNEL-positive cells are observed at or proximal to the CGZ. ONL, Outer nuclear layer; INL, inner nuclear layer; IPL, inner plexiform layer. ***B***, In whole mounts of retinas exposed to 6-OHDA 24 h previously, TUNEL-positive cells are sometimes evident within the depth of the neural retina (red arrows) but not at the CGZ. ***C***, In sections of retinas exposed to 6-OHDA 24 h previously, TUNEL-positive cells are sometimes (but rarely) encountered in the neural retina (red arrow) at a location in the INL that corresponds to the normal location of TH^+ somata.

about the location of any other heterotypic soma ($p > 0.05$; $n = 3$ retinas). Cross-correlational DRP analyses (cDRP) confirmed independence between the cellular patterns, with effective radius values that were always significantly lower than the corresponding values derived from the aDRP analyses ($p < 0.001$) (Table 1). In two of six comparisons, the cDRP-derived effective radius values were equal to zero, indicating the complete absence of a zone of exclusion between heterotypic cells. The cNND and cDRP analyses thus provide evidence that the 2D patterns of TH^+ and 5-HT^+ cells in goldfish retina, although nonrandom and sharing similar pattern attributes (e.g., local anticlustering), are not correlated with each other across 2D space (Cameron and Carney, 2004).

Evaluating cell death and migration as mechanisms of pattern formation

The observation of nonrandom independent cellular patterns across 2D space implied that cellular patterns emerge from the operation of one or more mechanisms that control, in a homotypic manner, the spatial arrangement of somata. Three candidate mechanisms for the formation of TH^+ and 5-HT^+ cellular patterns, spatiotemporal control of cell death, lateral migration, and spatiotemporal control of cell-fate decisions, were assessed.

If cell death contributes to cellular patterning, evidence of cell death would be expected at the CGZ, the spatial location of cellular patterning in this system. Additionally, based on the number of proliferative cells at the CGZ at any given time (Fig. 1*A*,*B*), the number of those cells that terminally differentiate (Fig. 1*C*), and the large number of different cell types in the fish retina (Yazulla and Studholme, 2001), a substantial number of cells exhibiting evidence of death would be expected. TUNEL-positive cells, however, were absent from the entirety of the CGZ of control and neurotoxin-exposed retinas ($n = 5$ retinas) (Fig. 3*A*,*B*). However, TUNEL-positive cells were observed outside the retina (Fig. 3*A*) or, in retinas exposed to neurotoxin, occasionally at the inner nuclear layer, corresponding to the location of the cell type targeted by the neurotoxin (Fig. 3*B*,*C*). Because TUNEL-positive cells were detected in this model system, the lack of such cells at, or proximal to, the CGZ suggested that neither retinal cytogenesis nor cellular pattern formation in the goldfish retina is substantially influenced by cell-death mechanisms.

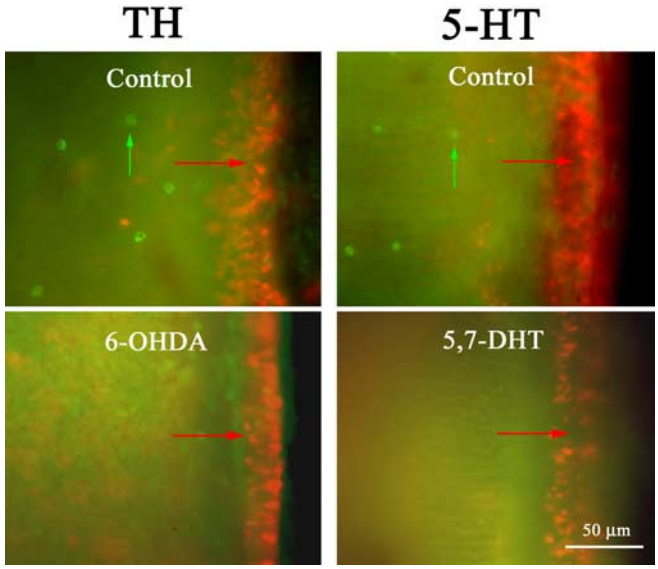

Figure 4. Neurotoxin-mediated cellular ablation. Three days after 6-OHDA, 5,7-DHT, or control solution exposure (BrdU only), retinas were screened for $BrdU^+$ cells (red arrows) and TH^+ or 5-HT^+ cells (green arrows). Note that TH^+ cells are absent from retinas exposed to 6-OHDA, and 5-HT^+ cells are absent from retinas exposed to 5,7-DHT.

During normal retinal growth, new cells are appositionally added to the retinal margin from the CGZ, which in turn progresses outward over time, leaving nonrandom cellular patterns in its "wake" (see supplemental figure, available at www.jneurosci.org as supplemental material). The presence and extent of cellular migration mechanisms during this process were evaluated by examining cellular patterns subsequent to selective ablation of specific retinal cell types (TH^+ or 5-HT^+). If lateral migration mechanisms contribute to cellular pattern formation during retinal growth, newly born cells would be expected to migrate into the ablated region (see supplemental figure, avail-

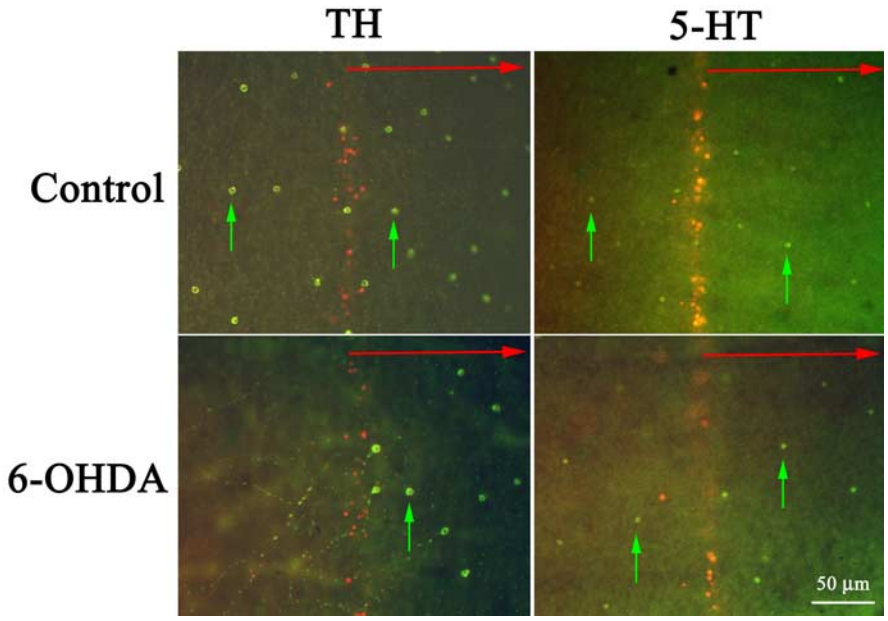

Figure 5. Cellular patterns 9 months after 6-OHDA exposure. In each panel, red arrows indicate the direction of retinal growth. Top, Control retinas indicating TH^+ and 5-HT^+ cells (green arrows) located central to (left of) and peripheral to (right of) the band of $BrdU^+$ cells. Bottom, Retinas exposed to 6-OHDA. TH^+ cells, the target of 6-OHDA, are absent from the central retina but are evident in the retina formed after the 6-OHDA exposure (i.e., to the right of the $BrdU^+$ band). The nontargeted cell type, 5-HT^+, was not affected by 6-OHDA (compare control retina).

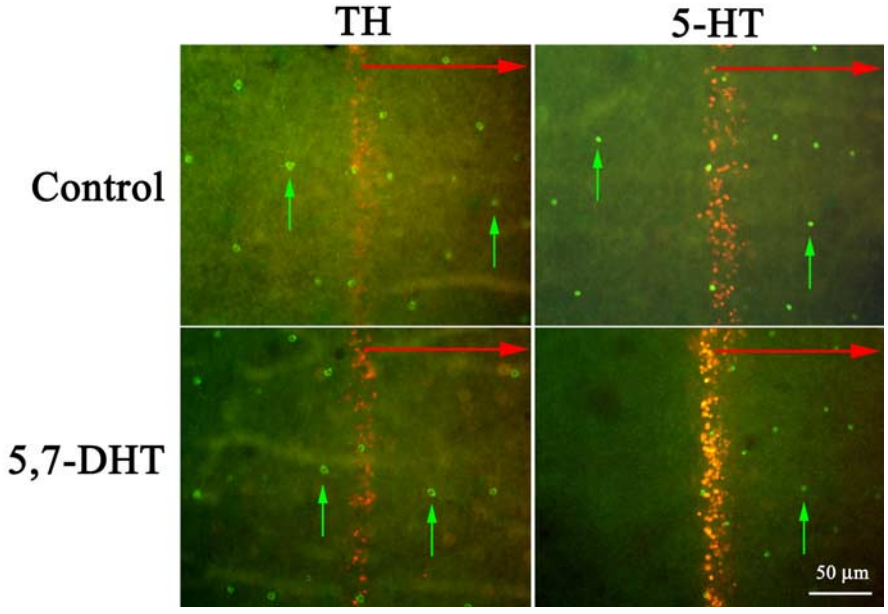

Figure 6. Cellular patterns 9 months after 5,7-DHT exposure. In each panel, red arrows indicate the direction of retinal growth. Top, Control retinas indicating TH^+ and 5-HT^+ cells (green arrows) located central to (left of) and peripheral to (right of) the band of $BrdU^+$ cells. Bottom, Retinas exposed to 5,7-DHT. 5-HT^+ cells, the target of 5,7-DHT, are absent from the central retina but are evident in the retina formed after the 5,7-DHT exposure (i.e., to the right of the $BrdU^+$ band). The nontargeted cell type, TH^+, was not affected by 5,7-DHT (compare control retina).

able at www.jneurosci.org as supplemental material), driven by hypothetical homotypic repelling signals that establish the homotypic zones of exclusion. A single intraocular administration of a neurotoxin (6-OHDA or 5,7-DHT; see Materials and Methods) successfully ablated >99% of cells of the target cell type, TH^+ or 5-HT^+, respectively (Fig. 4). Neurotoxin selectivity was indicated by the lack of ablation of the nontargeted cell type (see below). Neurotoxin exposure did not affect BrdU incorporation at the CGZ, as judged qualitatively by successful incorporation of BrdU, suggesting that undifferentiated progenitor cells at the CGZ were not targeted by the neurotoxins ($n = 13$ control and neurotoxin-exposed retinas each) (Fig. 4). Growth of retinas exposed to either 6-OHDA (Fig. 5, bottom) or 5,7-DHT (Fig. 6, bottom) was confirmed up to 9 months after neurotoxin exposure, with the amount of growth (assessed by the displacement of $BrdU^+$ cells into central retina) matching that observed in corresponding control retinas ($n = 15$ paired retinas; paired t test; $p > 0.26$) (Figs. 5, 6, top).

In retinas exposed to neurotoxin, there was no evidence for lateral migration of differentiated cells. Although cells of the targeted type were generated subsequent to neurotoxin exposure, up to 9 months later, none of these somata were located in the ablated region; that is, central and nonadjoining to the band of $BrdU^+$ cells, which demarcates the location of the CGZ at the time of neurotoxin exposure (Figs. 5, 6). If lateral migration of differentiated cells was a dominant mechanistic determinant of the physical attributes of the cellular patterns (for example, local anticlustering), newly generated cells would be expected to migrate into that region of the retina denuded of the homotypic cell type (see Discussion and supplemental material, available at www.jneurosci.org).

Evidence for the operation of mechanisms that spatiotemporally control cell-fate decisions at the CGZ was observed. An atypical increase in the density of the neurotoxin-targeted cell types was observed immediately distal to the band of $BrdU^+$ cells (Fig. 7). This increase in density, which was present within the first 20 μm of new retinal growth after neurotoxin exposure, was statistically significant for both TH^+ and 5-HT^+ cells ($p < 0.01$ and 0.003, respectively; $n = 7$ and 6 retinas for each condition, respectively). Because of the appositional nature of cellular addition from the CGZ, the region of higher density corresponds to the location in which neurogenesis occurred immediately after neurotoxin exposure (Figs. 4–6). The cell density function in the neurotoxin-treated retina peaked at a location just distal to the BrdU labeling and at more distal locations (Fig. 7, abscissa values >0) was not different from that of control retina. This density profile indicated, subsequent to BrdU incorporation, a greater number of the targeted cell type in the neurotoxin-treated retinas compared with control, suggesting that the elevated density was attributable to an induced transient hyperplasia and to atypical cellular migration (for example, the region of elevated density

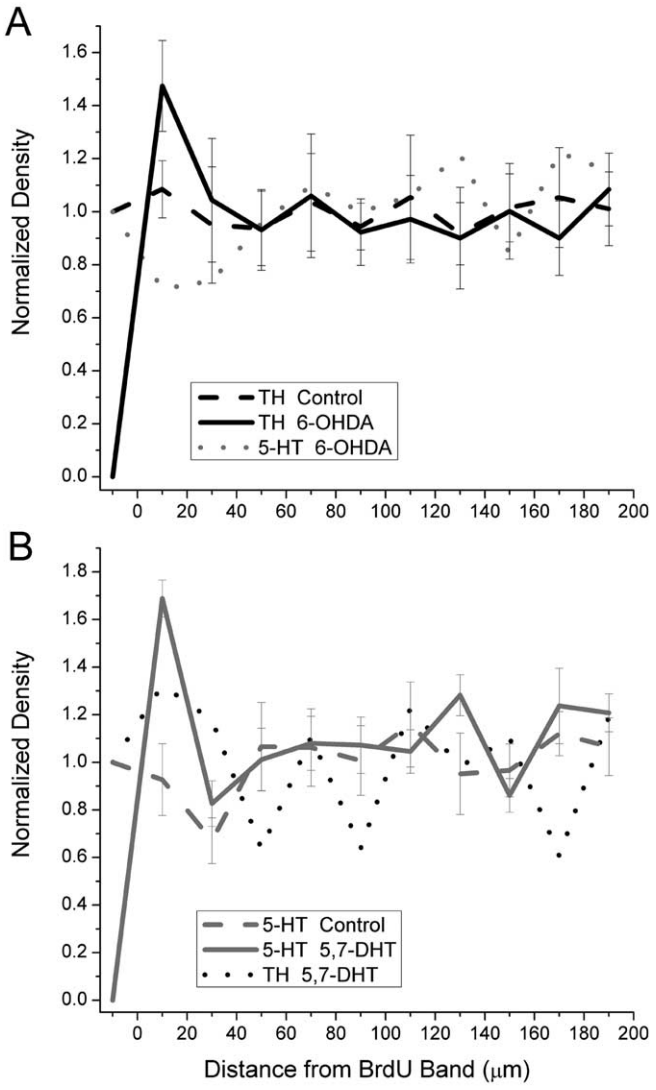

Figure 7. Normalized cell densities of neurotoxin-targeted and nontargeted cell types during retinal growth after neurotoxin exposure. The position of the BrdU$^+$ band of cells is defined as abscissa value 0.0. Plotted values are mean ± SE. Top, Normalized cell densities of TH$^+$ cells (black lines) in control retinas (dashed line; $n = 6$) and retinas exposed to 6-OHDA (solid line; $n = 6$) and 5-HT$^+$ cells in retinas exposed to 6-OHDA (gray dotted line; $n = 2$). There is a statistically significant elevation in TH$^+$ cells within 20 μm of the BrdU$^+$ band (see Results). Bottom, Normalized cell densities of 5-HT$^+$ cells (gray lines) in control retinas (dashed line; $n = 6$) and retinas exposed to 5,7-DHT (solid line; $n = 6$) and TH$^+$ cells in retinas exposed to 5,7-DHT (black dotted line). There is a statistically significant elevation in 5-HT$^+$ cells within 20 μm of the BrdU$^+$ band (see Results). Error bars represent SEM.

being populated by cells that migrated to that location from some other region). Because there was no corresponding statistically significant increase in the density of the nontargeted cell type (Fig. 7), the transient hyperplasia was likely to be cell-type specific. Furthermore, the persistence of the elevated cellular density throughout the growth period, which extended to 9 months, provided additional indirect evidence that neither cell death nor lateral migration were significant patterning mechanisms; that is, neither cell death nor migration mechanisms ultimately "pruned" the hyperplastic region to the "appropriate" cellular density (Fig. 7).

The cellular patterns of both TH$^+$ and 5-HT$^+$ cells formed subsequent to their respective hyperplasia were not significantly different from those of corresponding control retinas. With respect to cellular density, at distances of new growth >20 μm from the BrdU$^+$ band, there was no significant difference between ablated and control retinas ($p > 0.3$ for distances from 20 to 140 μm for both TH$^+$ and 5-HT$^+$ cells derived from seven and six retina pairs, respectively) (Fig. 7). Similarly, the NND distributions of TH$^+$ and 5-HT$^+$ patterns in control and postablation retina were not significantly different ($p > 0.1$ for both TH$^+$ and 5-HT$^+$ cells derived from five and four retina pairs, respectively). Quadrat analysis of the TH$^+$ and 5-HT$^+$ patterns revealed that all of the patterns in ablated and control retinas were regular (data not shown). DRP analysis also revealed no significant differences between the patterns: expressed as a percentage, the effective radius values for TH$^+$ and 5-HT$^+$ patterns in their respective ablated retinas differed by +5.2 ± 14.7 and +0.8 ± 24.2% of the corresponding control values ($n = 5$ and 4 retina pairs, respectively). These results indicated a posthyperplasia resumption/restoration of the nominal regulation of cell number and patterning during retinal growth.

A computational model predicts normal and experimental cellular pattern formation

Because cell death and lateral migration mechanisms were apparently not dominant contributors to pattern formation in this model system, the role of spatiotemporal control of cell-fate decisions at the CGZ was further evaluated. A computational model of this mechanism has been developed (Cameron and Carney, 2004) (see Materials and Methods and supplemental material, available at www.jneurosci.org), and its ability to predict cellular pattern formation in control and experimental goldfish retina was tested.

The computational model accurately predicted cellular pattern formation in control goldfish retinas out to 9 months after BrdU exposure. For both TH$^+$ and 5-HT$^+$ cell types, a value of the model parameter λ (the space constant of the signaling mechanism, arising from differentiated cells, that inhibited homotypic cell fates) was identified that generated model-derived patterns with NND distributions that were not significantly different from those of the corresponding seed (Fig. 8, top, Table 2) ($p > 0.1$ for TH$^+$ and 5-HT$^+$ cells; $n = 18$ and 15 pattern pairings, respectively). Poor matches between the seed and model-derived patterns were, however, readily achieved with values of λ above or below the identified value (data not shown). For both TH$^+$ and 5-HT$^+$ cells, the value of λ used in the simulations was similar to the aNNDs for the seed data, with λ/NND varying between 1.00 and 1.14, similar to that derived for modeled pattern formation of TH$^+$ and 5-HT$^+$ cells in zebrafish retina (Cameron and Carney, 2004). Quadrat analysis revealed that all of the model-derived patterns matched the corresponding seed in being regular (Fig. 8, middle). Furthermore, DRP analysis indicated that the effective radius values for the seed and model-derived patterns were not significantly different ($p > 0.6$ and 0.2 for TH$^+$ and 5-HT$^+$ cells, respectively) (Table 2). These results indicated that a homotypic signaling mechanism that controls cell-fate decisions at the CGZ recapitulates qualitative and quantitative aspects of cellular patterns in the normal goldfish retina.

The computational model was also tested for its ability to predict the effects of targeted cellular ablation after subsequent pattern formation; specifically, the transient hyperplasia and subsequent restoration of the normal homotypic pattern (Fig. 7). In the model, progenitor cells at the CGZ, freed from the homotypic inhibitory signal arising from central retina, transiently (i.e.,

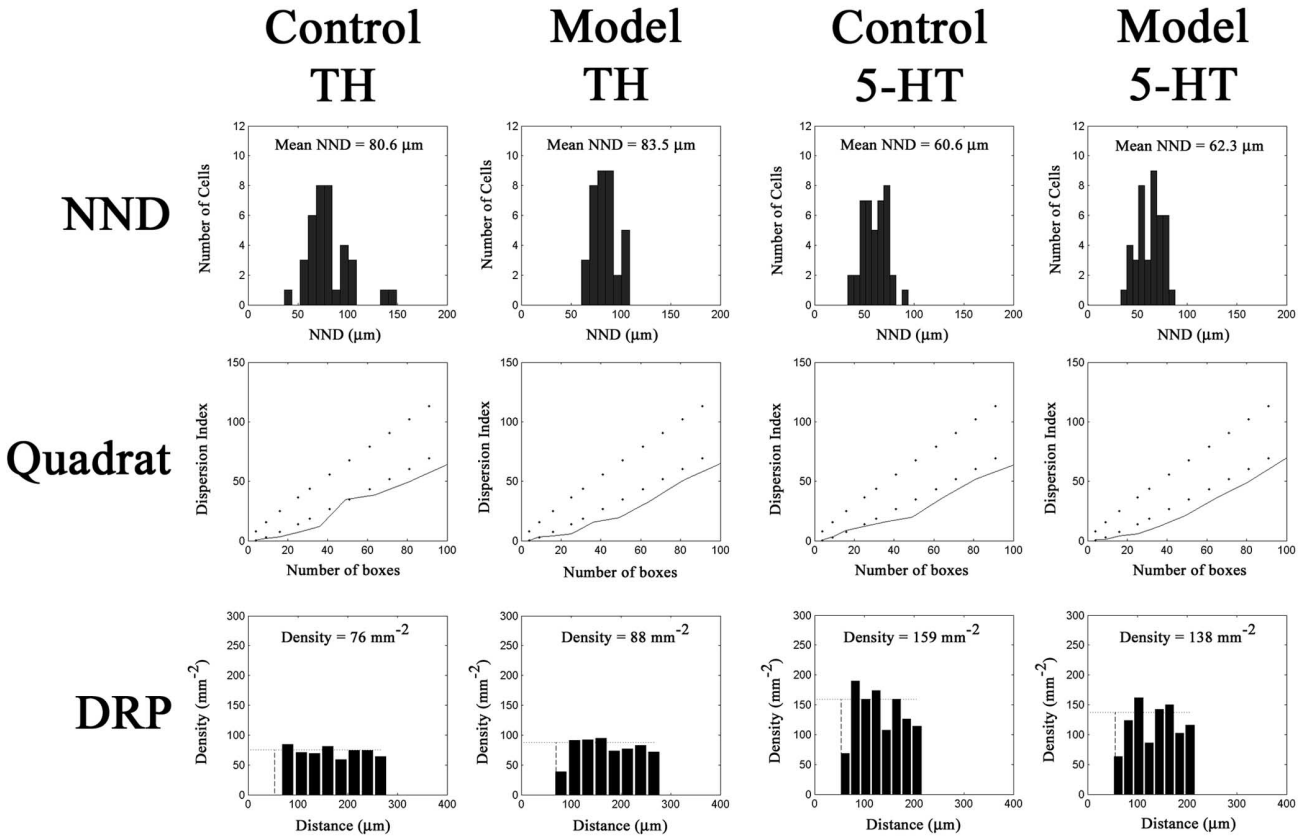

Figure 8. Spatial pattern analysis of TH$^+$ and 5-HT$^+$ cellular patterns *in vivo* and in modeled control retinal growth. NND (top), quadrat (middle), and DRP (bottom) analyses of a representative TH$^+$ (Control TH) and 5-HT$^+$ (Control 5-HT) cellular pattern are shown. These patterns served as the seed for the corresponding model-derived patterns (Model TH and Model 5-HT). Mean NND values and recovered cell densities from the DRP analysis are indicated; in the DRP plots, the recovered cell density is indicated graphically by the horizontal dotted line, and the effective radius is indicated by the vertical dashed line. The quadrat functions, which mostly lie below the central demarcated field of each plot, indicate cellular patterns that exhibit long-range regularity (rather than aggregation or randomness) (Grieg-Smith, 1964; Stenkamp et al., 2001; Cameron and Carney, 2004). Note the overall similarity between the *in vivo* and model-derived patterns (see Results) (Tables 1, 2).

proximal to the BrdU$^+$ band) increased the number of targeted cells that were produced (see supplemental figure, available at www.jneurosci.org as supplemental material). The inhibitory signaling mechanism of the model was defined as being homotypic, which conceptually matches the apparent homotypic effects of the neurotoxins (Figs. 5–8).

For both TH$^+$ and 5-HT$^+$ cells, the computational model recapitulated both the transient hyperplasia of the targeted cell type and the subsequent restoration of the normal cellular pattern in ablated retina. In the model, removal of the homotypic inhibitory signal resulted in undifferentiated cells at the CGZ being more likely to differentiate into the ablated cell phenotype, and this was manifested, for both TH$^+$ and 5-HT$^+$ cells, as an approximately threefold increase in cellular density proximal to the denuded retina compared with control (Fig. 9). This elevation in cellular density was similar to, but approximately twofold greater than, the observed *in vivo* hyperplasia (compare Fig. 9, solid blue and red lines) (see Discussion). The posthyperplasia restoration of the normal cellular density was evident as densities that, at distances >50 μm from the BrdU$^+$ band, were not significantly different between the control and neurotoxin-exposed model patterns ($p > 0.15$; $n = 2$ sets of seed data from each of nine control retinas labeled for TH$^+$ cells and five model simulations for each set) (Fig. 9). Similarly, there were no significant differences in the NND distributions for model-derived patterns generated in the presence or absence of a seed, the latter analyzed subsequent to the transient hyperplasia ($p > 0.7$ and 0.5 for TH$^+$ and 5-HT$^+$ cells, respectively) (Table 2, Fig. 10, top). The quadrat analyses of these patterns revealed no significant differences (Fig. 10), and DRP analysis indicated that the effective radius values were not significantly different ($p > 0.8$ and 0.2 for TH$^+$ and 5-HT$^+$ cells, respectively) (Table 2). These results indicated that the computational model, which used a homotypic cell-fate control mechanism, was able to recapitulate qualitative and quantitative aspects of both the typical cellular pattern formation of control retina and the atypical cellular pattern formation associated with targeted ablation of differentiated cells.

Discussion

Regularity and independence of TH$^+$ and 5-HT$^+$ cell patterns in goldfish retina

The high degree of cellular order in the vertebrate retina provides an important structural basis for its functional characteristics (Wässle and Riemann, 1978; Wässle et al., 1983; Galli-Resta, 1998, 2000; Raven and Reese, 2002). The observation that cells in the vertebrate retina are arranged nonrandomly across two-dimensional space was originally reported by Hannover (1840), and a large number of subsequent investigations have confirmed this cellular attribute of the vertebrate retina (Eigenmann and

Table 2. NND and DRP analyses of empirical and model-derived patterns of TH^+ and 5-HT^+ cells for control and neurotoxin-exposed retinas

Cell type	Data aNND (μm)	Data aR_{eff} (μm)	Model control aNND (μm)	Model control aR_{eff} (μm)	Model ablated aNND (μm)	Model ablated aR_{eff} (μm)
TH	80.9 ± 20.0 (28)	54.2	77.3 ± 10.6 (42)	66.0	76.7 ± 18.5 (30)	71.4
			79.1 ± 14.2 (23)	82.3	73.1 ± 13.8 (26)	65.1
			75.2 ± 11.6 (34)	75.5	77.4 ± 17.9 (29)	71.4
TH	76.2 ± 12.2 (24)	72.2	74.3 ± 16.7 (27)	62.7	79.1 ± 15.3 (21)	67.8
			77.2 ± 15.6 (16)	63.2	78.8 ± 13.8 (43)	70.5
			73.7 ± 15.1 (30)	77.1	75.7 ± 13.3 (50)	88.5
TH	82.8 ± 21.0 (24)	81.6	81.5 ± 16.1 (30)	75.2	81.8 ± 20.6 (31)	81.7
			81.8 ± 12.9 (27)	75.7	81.2 ± 17.7 (30)	77.8
			83.8 ± 12.9 (27)	86.5	83.2 ± 17.4 (34)	82.7
TH	64.3 ± 15.9 (34)	61.0	65.0 ± 13.8 (35)	68.0	71.0 ± 11.6 (34)	61.7
			69.3 ± 13.8 (27)	60.9	74.1 ± 14.6 (52)	66.6
			69.7 ± 14.4 (25)	57.9	69.2 ± 16.7 (37)	61.0
TH	86.5 ± 27.6 (24)	90.7	88.4 ± 17.9 (24)	78.7	82.6 ± 26.5 (19)	72.3
			82.9 ± 18.8 (19)	89.9	81.7 ± 17.0 (29)	73.7
			85.8 ± 16.1 (18)	81.9	85.9 ± 17.0 (29)	80.2
TH	93.3 ± 22.9 (24)	71.0	86.9 ± 18.1 (29)	66.7	87.3 ± 22.3 (21)	75.8
			94.1 ± 21.1 (24)	80.6	89.8 ± 22.0 (23)	75.7
			83.4 ± 17.2 (20)	84.4	93.6 ± 22.0 (30)	82.6
5-HT	62.0 ± 12.7 (42)	57.0	62.2 ± 14.3 (32)	52.0	61.7 ± 12.7 (60)	56.7
			63.5 ± 12.2 (42)	57.3	63.5 ± 18.1 (57)	59.7
			60.4 ± 12.5 (38)	58.9	65.9 ± 10.8 (25)	57.9
5-HT	50.5 ± 12.4 (48)	43.3	50.1 ± 9.6 (51)	48.1	49.1 ± 11.3 (39)	43.7
			51.9 ± 8.3 (47)	73.2	50.9 ± 8.8 (42)	41.8
			48.8 ± 11.8 (47)	51.3	52.4 ± 10.5 (37)	48.9
5-HT	52.9 ± 11.5 (76)	42.8	55.5 ± 10.4 (68)	43.5	55.5 ± 12.2 (126)	44.8
			51.7 ± 11.1 (76)	46.9	57.9 ± 11.5 (121)	47.5
			54.7 ± 12.0 (68)	47.7	55.1 ± 12.1 (80)	47.7
5-HT	63.8 ± 14.2 (41)	52.7	58.9 ± 11.4 (85)	59.9	58.9 ± 11.4 (85)	59.1
			62.3 ± 17.3 (45)	57.7	66.2 ± 12.9 (61)	49.8
			61.2 ± 14.5 (45)	55.6	64.7 ± 11.4 (60)	51.4
5-HT	58.0 ± 14.7 (36)	50.8	61.3 ± 16.9 (36)	53.2	57.6 ± 9.7 (51)	42.9
			59.8 ± 11.3 (30)	43.6	58.0 ± 12.5 (38)	54.7
			60.1 ± 9.1 (25)	53.6	60.2 ± 12.5 (46)	51.6

In each row, the cell type is indicated; NND and effective radius values are presented as mean ± SD (number of cells). Data were derived from retinas exposed to BrdU alone (control) and served as the seed for the "Model control" condition (results from 3 model simulations of control growth, using the same data seed, are indicated). "Model ablated" refers to simulations in which the seed was removed to mimic *in vivo* ablation. The λ values derived from the Model control simulations were used in the corresponding Model ablated condition (see Materials and Methods). Symbols and abbreviations are as in Table 1.

Shafer, 1900; Lyall, 1957; Engström, 1963; Marc and Sperling, 1976; Williams, 1988; Wikler and Rakic, 1990; Wässle and Boycott, 1991; Cameron and Easter, 1993; Vaney, 1994; Cook, 1996; Cameron and Carney, 2000, 2004; Cook and Chalupa, 2000; Galli-Resta, 2000; Rockhill et al., 2000; Stenkamp et al., 2001).

In an effort to identify and characterize the determinants of these nonrandom cellular patterns, we took advantage of the goldfish retina as a model system. The goldfish retina grows throughout life by the appositional addition of new cells at the retinal margin (Fig. 1) (Johns, 1977; Kock, 1982), thus providing an identifiable, accessible, and geometrically well defined substrate against which alternative mechanisms of cellular pattern formation such as cell death, lateral migration, and cell-fate decision could be directly evaluated. Additionally, TH^+ and 5-HT^+ cells in the goldfish inner retina are arrayed nonrandomly and independently across 2D space (Fig. 2), thus providing well characterized patterns for evaluating formation mechanisms. Finally, TH^+ and 5-HT^+ cells in the retina, as confirmed here, can be selectively ablated by exposure to specific neurotoxins (Fig. 4) (Dowling and Ehinger, 1978; Negishi et al., 1982, 1985; Watling et al., 1982; Reh and Tully, 1986; McAvoy and Chamberlain, 1990; Braisted and Raymond, 1993; Hitchcock and Vanderyt, 1994; Yazulla and Studholme, 1997; Raven et al., 2003), thus enabling the direct testing of hypotheses regarding the contribution of

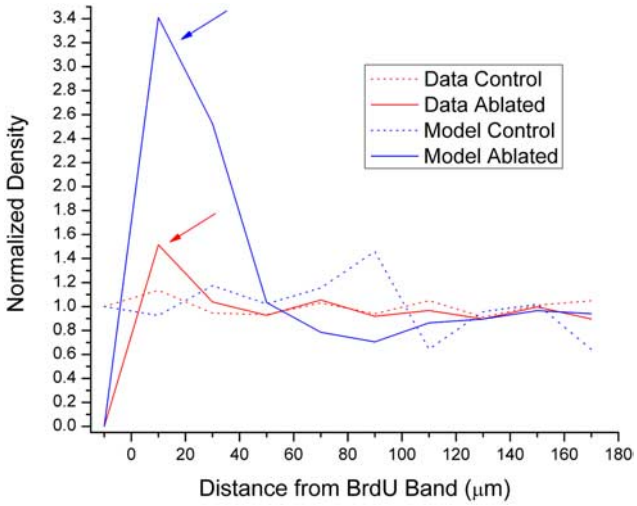

Figure 9. Empirically observed (red) and model-derived predictions (blue) of normalized cellular densities in control and neurotoxin-exposed retina. Using TH^+ cells as the illustrated example, the predicted cellular densities for control (dotted lines) and ablated (solid lines) conditions are plotted as a function of distance from the $BrdU^+$ band of cells, and the latter is defined as abscissa value 0.0. Note in the experimental conditions the lack of cells central to the $BrdU^+$ band, the elevated density of cells in the region of new growth immediately adjacent to the $BrdU^+$ band (arrows), and the ultimate resumption of the control density. The differential amplitude of hyperplasia between the model and empirical data is considered in Discussion.

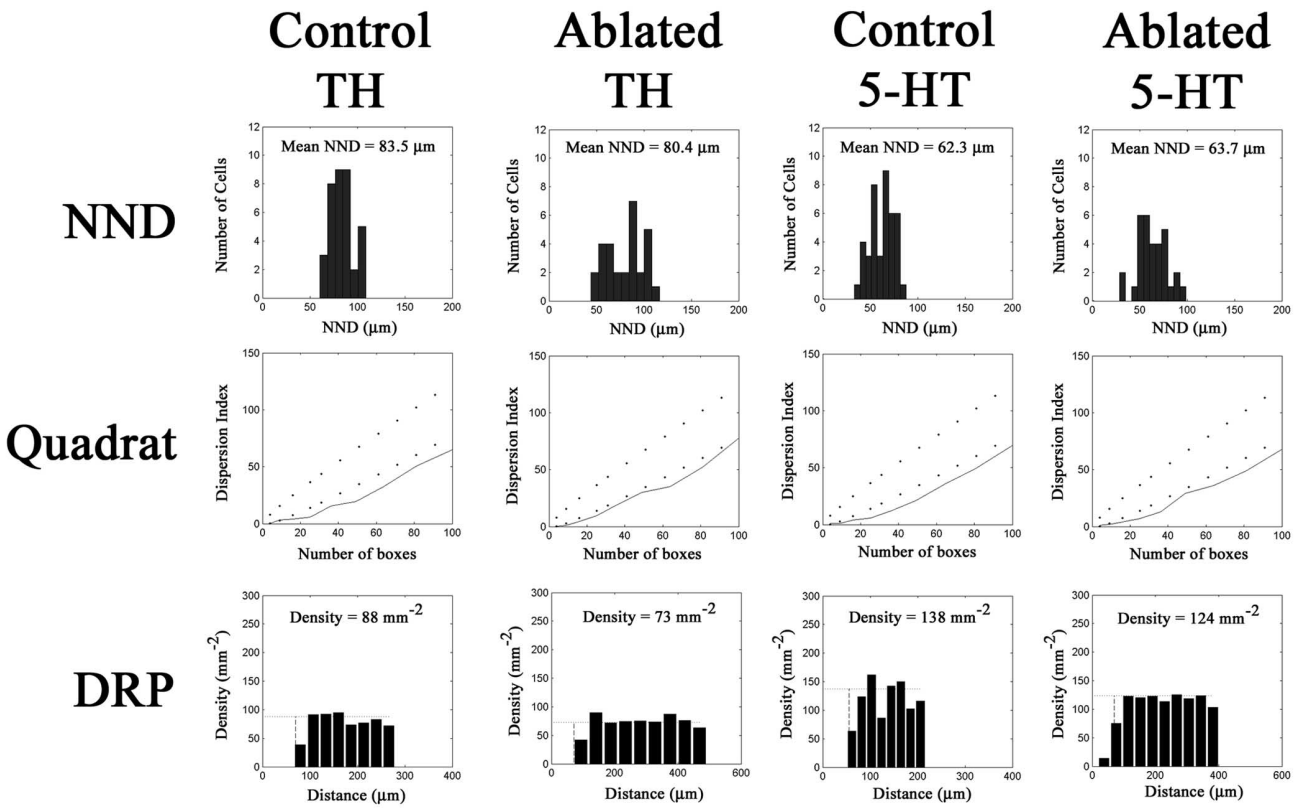

Figure 10. Spatial analyses of model-derived cellular patterns for control and neurotoxin-ablated retinas. NND (top), quadrat (middle), and DRP (bottom) analyses of representative model-derived TH$^+$ and 5-HT$^+$ cellular patterns in control (Control TH and Control 5-HT), 6-OHDA-exposed (Ablated TH), and 5,7-DHT-exposed (Ablated 5-HT) retinas are shown. Mean NND values, quadrat function, and DRP functions are indicated as in Figure 8. In the ablated conditions, the region of hyperplasia was excluded. Note the overall similarity between the control and neurotoxin-exposed model-derived patterns (see Results) (Table 2).

differentiated cells in providing instructive cues that guide cellular pattern formation during retinal growth.

Cell death and lateral migration mechanisms do not dominate TH$^+$ and 5-HT$^+$ pattern formation

Nonrandom cellular patterns could be established via multiple mechanisms, including regulation of cell death, lateral migration of cells, or spatiotemporal regulation of cell-fate decisions. Our empirical evidence suggested that the patterns of TH$^+$ and 5-HT$^+$ cells in goldfish retina are not formed via spatiotemporal regulation of cell death. Although TUNEL-positive cells were readily detected, there was no evidence for such cells at the CGZ (Fig. 3), the site at which cell death, if it was controlling cellular patterning, would be expected to be observed. Furthermore, in retinas exposed to neurotoxin, the long-term persistence of localized regions of hyperplasia indicated that cell-death mechanisms did not ultimately prune these atypical patterns into more appropriate patterns.

A substantial role for lateral migration was ruled out by the lack of evidence for migration of TH$^+$ or 5-HT$^+$ cells into regions of retina denuded of the homotypic cell, even up to 9 months after cellular ablation (Figs. 5, 6). If lateral migration of somata had occurred, particularly a migration driven by homotypic mutual-repelling mechanisms, the most favorable migratory direction would have been into the denuded region (attributable to its lower total complement of cells, this region should also have provided a more advantageous microenvironment for migration than normal retina). Lateral migration mechanisms could also not account for the transient elevation in TH$^+$ and 5-HT$^+$cell production subsequent to their ablation, and the long-term persistence of hyperplastic regions indicated that cells within these regions of atypical patterning did not redistribute themselves into more appropriate patterns, via migration into either the denuded retina or the retina formed subsequent to ablation. The combined lack of evidence for cell death at the CGZ and the apparent absence of lateral migration of differentiated cells indicated the operation of some other mechanism(s) for controlling cellular pattern formation in this system.

Evidence that pattern formation is dominated by spatiotemporal control of cell-fate decisions

A computational model of cellular pattern formation suggested that a mechanism that controls cell-fate decisions at the CGZ could account for cellular pattern formation in this system. Using a signaling mechanism, arising from differentiated cells, that inhibited the formation of homotypic cells, the model accurately predicted quantitative aspects of TH$^+$ and 5-HT$^+$ cellular patterns in control retina, as determined by NND, DRP, and quadrat analyses (Fig. 8, Table 2). Additionally, and perhaps most importantly, using the same parameter values as those used for control retinal growth, for both cell types, the model accurately predicted the transient hyperplasia and the subsequent restoration of the normal cellular patterns after selective cellular ablation (Fig. 10).

The spatial attributes of TH$^+$ and 5-HT$^+$ cellular patterns argued against alternative signaling schemes for controlling cell-

fate decisions. Because they are homotypically anticlustered, the operation of a homotypic promotive signal for controlling cell-fate decisions was ruled out, because such a strategy would generate aggregated patterns that do not exhibit homotypic zones of exclusion. Additionally, because the 2D patterns of TH^+ and 5-HT^+ cells are independent (as are other inner retinal cell types) (Cameron and Carney, 2004), the contribution of heterotypic promotive signaling is questionable. Such signaling would generate cellular patterns that are spatially correlated in some nonrandom manner, yet no such spatial correlation was observed. Although the operation of promotive signaling strategies cannot be formally ruled out, the spatial characteristics of the observed cellular patterns, as derived from autocorrelational and cross-correlational analyses, indicate that homotypic inhibitory signaling mechanisms are parsimonious.

The statistically significant, transient, cell-type-specific hyperplasia that occurred during retinal growth subsequent to neurotoxin exposure was similar to that reported previously (Negishi et al., 1982; Reh and Tully, 1986; Li and Dowling, 2000). That the hyperplasia was limited to the ablated cell type was consistent with a lack of heterotypic inductive or instructive patterning cues between TH^+ and 5-HT^+cells, although the somata of both cell types occupy the inner nuclear layer. Spatial pattern analysis revealed that cellular patterns formed subsequent to hyperplasia did not differ from those of corresponding control retina (Fig. 10, as predicted by the computational model), indicating an ultimate resumption/restoration of the mechanism(s) that controls the number and patterns of differentiated cells.

We hypothesize that compared with the situation *in vivo*, the greater predicted hyperplasia of the model (Fig. 9) was attributable to an overestimate of the number of progenitor cells within the CGZ that could differentiate into the TH^+ or 5-HT^+ phenotypes. The model assumed that all proliferative cells within the CGZ could differentiate into the seed cell type. Although we are currently unable to define the number of progenitors that, at any given time, are competent to differentiate into TH^+ or 5-HT^+ cells, the model results suggest that not all proliferative cells in the CGZ have equivalent lineage potential.

Hypothesized signaling mechanisms for controlling cell-fate decisions in the growing retina

The success of the model in simulating the formation of cellular patterns raises the question of the underlying molecular basis. The physical characteristics of instructive signals that are known to affect cell-fate decisions in the retina are varied and include cell-surface signaling (Link et al., 2000; Scheer et al., 2001) and diffusible agents (Altshuler and Cepko, 1992; Hicks and Courtois, 1992; Watanabe and Raff, 1992; Hyatt et al., 1996; Neumann and Nuesslein-Volhard, 2000; Stenkamp et al., 2000). Additionally, there is ample evidence for the operation of signals that inhibit, at some level, the production of retinal cells (Negishi et al., 1982; Reh and Tully, 1986; Hewitt et al., 1990; Hunter et al., 1992; Lillien, 1995; Ezzeddine et al., 1997; Fadool et al., 1997; Levine et al., 1997; Neophytou et al., 1997; Waid and McLoon, 1998; Belliveau and Cepko, 1999; Malicki and Driever, 1999; Doerre and Malicki, 2001; Jensen et al., 2001; Kay et al., 2001; Frankfort and Mardon, 2002). The computational model used in this study provides physical constraints to which any hypothesized molecular signaling mechanism must adhere: it must operate over a spatial scale that extends considerably beyond the soma size, and it must operate in a homotypic manner. The latter constraint might rule out agents known to target multiple cell types, such as retinoic acid (Hyatt et al., 1996) or sonic hedgehog (Neumann and Nuesslein-Volhard, 2000).

We hypothesize that neurotransmitters could mediate the homotypic inhibitory signaling implied by our results. Several attributes of neurotransmitters and their signaling mechanisms make them attractive candidates: they provide a basis for cell-type specificity; plausible mechanisms for neurotransmitter delivery have been reported, including volume transmission of molecules released from a synaptic apparatus (Mora-Ferrer et al., 1999; Cragg and Rice, 2004); neurotransmitters can activate complex intracellular signaling cascades, potentially resulting in changes in gene transcription (Paspalas and Goldman-Rakic, 2004); neurotransmitters are known to regulate various aspects of cellular development (Lankford et al., 1988; Rodrigues et al., 1990; Jung and Bennett, 1996; Lima et al., 1996; Buznikov et al., 1999; Moiseiwitsch, 2000; Zachor et al., 2000; Herlenius and Lagercrantz, 2001). Direct evaluation of the neurotransmitter hypothesis of cell-fate determination and cellular pattern formation in the growing goldfish retina is the subject of ongoing investigation.

References

Altshuler D, Cepko C (1992) A temporally regulated, diffusible activity is required for rod photoreceptor development *in vitro*. Development 114:947–957.

Belliveau MJ, Cepko CL (1999) Extrinsic and intrinsic factors control the genesis of amacrine and cone cells in the rat retina. Development 126:555–566.

Braisted JE, Raymond PA (1993) Continued search for the cellular signals that regulate regeneration of dopaminergic neurons in goldfish retina. Brain Res Dev Brain Res 76:221–232.

Buznikov GA, Shmukler YB, Lauder JM (1999) Changes in the physiological roles of neurotransmitters during individual development. Neurosci Behav Physiol 29:11–21.

Cameron DA (1995) Asymmetric retinal growth in the adult teleost green sunfish (*Lepomis cyanellus)*. Vis Neurosci 12:95–102.

Cameron DA, Carney LH (2000) Cell mosaic patterns in the native and regenerated inner retina of zebrafish; implications for retinal assembly. J Comp Neurol 416:356–367.

Cameron DA, Carney LH (2004) Cellular patterns in the inner retina of adult zebrafish: quantitative analyses and a computational model of their formation. J Comp Neurol 471:11–25.

Cameron DA, Easter Jr SS (1993) The cone photoreceptor mosaic of the green sunfish, *Lepomis cyanellus*. Vis Neurosci 10:375–384.

Cameron DA, Easter Jr SS (1995) Cone photoreceptor regeneration in adult fish retina: phenotypic determination and mosaic pattern formation. J Neurosci 15:2255–2271.

Cook JE (1996) Spatial properties of retinal mosaics: an empirical evaluation of some existing measures. Vis Neurosci 13:15–30.

Cook JE, Chalupa LM (2000) Retinal mosaics: new insights into an old concept. Trends Neurosci 23:26–34.

Cragg SJ, Rice ME (2004) DAncing past the DAT at a DA synapse. Trends Neurosci 27:270–277.

Cusato K, Stagg SB, Reese BE (2001) Two phases of increased cell death in the inner retina following early elimination of the ganglion cell population. J Comp Neurol 439:440–449.

Doerre G, Malicki J (2001) A mutation of early photoreceptor development, *mikre oko*, reveals cell–cell interactions involved in the survival and differentiation of zebrafish photoreceptors. J Neurosci 21:6745–6757.

Dowling JE, Ehinger B (1978) The interplexiform cell system. I. Synapses of the dopaminergic neurons of the goldfish retina. Philos Trans R Soc Lond B Biol Sci 201:7–26.

Easter Jr SS (1992) Retinal growth in foveated teleosts: nasotemporal asymmetry keeps the fovea in temporal retina. J Neurosci 12:2381–2392.

Eglen SJ, Willshaw DJ (2002) Influence of cell fate mechanisms upon retinal mosaic formation: a modelling study. Development 129:5399–5408.

Eglen SJ, van Ooyen A, Willshaw DJ (2000) Lateral cell movement driven by

dendritic interactions is sufficient to form retinal mosaics. Network 11:103–118.
Eigenmann CH, Shafer GD (1900) The mosaic of single and twin cones in the retina of fishes. Am Nat 34:109–118.
Engström K (1963) Cone types and cone arrangements in teleost retinas. Acta Zool 44:179–243.
Ezzeddine ZD, Yang X, DeChiara T, Yancopoulos G, Cepko CL (1997) Postmitotic cells fated to become rod photoreceptors can be respecified by CNTF treatment of the retina. Development 124:1055–1067.
Fadool JM, Brockerhoff SE, Hyatt GA, Dowling JE (1997) Mutations affecting eye morphology in the developing zebrafish (*Danio rerio*). Dev Genet 20:288–295.
Frankfort BJ, Mardon G (2002) R8 development in the *Drosophila* eye: a paradigm for neural selection and differentiation. Development 129:1295–1306.
Galli-Resta L (1998) Patterning the vertebrate retina: the early appearance of retinal mosaics. Semin Cell Dev Biol 9:279–284.
Galli-Resta L (2000) Local, possible contact-mediated signalling restricted to homotypic neurons controls the regular spacing of cells within the cholinergic arrays in the developing rodent retina. Development 127:1509–1516.
Galli-Resta L, Resta G, Tan SS, Reese BE (1997) Mosaics of islet-1-expressing amacrine cells assembled by short-range cellular interactions. J Neurosci 17:7831–7838.
Grieg-Smith P (1964) Quantitative plant ecology, Chap 3, Ed 2. London: Butterworths.
Hannover A (1840) Ueber die Netzhaut und ihre Gehirnsubstanz bei Wirbelthieren, mit Ausnahme des Menschen. Archiv für Anatomie, Physiologie und Wissenschaftliche Medicin 320–345.
Hendrickson AE (1994) Primate foveal development: a microcosm of current questions in neurobiology. Invest Ophthalmol Vis Sci 35:3129–3133.
Herlenius E, Lagercrantz H (2001) Neurotransmitters and neuromodulators during early human development. Early Hum Dev 65:21–37.
Hewitt AT, Lindsey JD, Carbott D, Adler R (1990) Photoreceptor survival-promoting activity in interphotoreceptor matrix preparations: characterization and partial purification. Exp Eye Res 50:79–88.
Hicks D, Courtois Y (1992) Fibroblast growth factor stimulates photoreceptor differentiation *in vitro*. J Neurosci 12:2022–2033.
Hitchcock PF, Vanderyt JT (1994) Regeneration of the dopamine-cell mosaic in the retina of the goldfish. Vis Neurosci 11:209–217.
Hunter DD, Murphy MD, Olsson CV, Brunken WJ (1992) S-laminin expression in adult and developing retinae: a potential cue for photoreceptor morphogenesis. Neuron 8:399–413.
Hyatt GA, Schmitt EA, Fadool JM, Dowling JE (1996) Retinoic acid alters photoreceptor development in vivo. Proc Natl Acad Sci USA 93:13298–13303.
Jensen AM, Walker C, Westerfield M (2001) mosaic eyes: a zebrafish gene required in pigmented epithelium for apical localization of retinal cell division and lamination. Development 128:95–105.
Jeyarasasingam G, Snider CJ, Ratto GM, Chalupa LM (1998) Activity-regulated cell death contributes to the formation of ON and OFF alpha ganglion cell mosaics. J Comp Neurol 394:335–343.
Johns PR (1977) Growth of the adult goldfish eye. III. Source of the new retinal cells. J Comp Neurol 176:343–358.
Jung AB, Bennett JP (1996) Development of striatal dopaminergic function. III. Pre- and postnatal development of striatal and cortical mRNAs for the neurotrophin receptors trkBTK+ and trkC and their regulation by synaptic dopamine. Brain Res Dev Brain Res 94:133–143.
Kay JN, Finger-Baier KC, Roeser T, Staub W, Baier H (2001) Retinal ganglion cell genesis requires *lakritz*, a zebrafish *atonal* homolog. Neuron 30:725–736.
Kock J-H (1982) Neuronal addition and retinal expansion during growth of the crucian carp eye. J Comp Neurol 209:264–274.
Lankford KL, DeMello FG, Klein WL (1988) D1-type dopamine receptors inhibit growth cone motility in cultured retina neurons: evidence that neurotransmitters act as morphogenetic growth regulators in the developing central nervous system. Proc Natl Acad Sci USA 85:2839–2843.
Levine EM, Passini M, Hitchcock PF, Glasgow E, Schechter N (1997) Vsx-1 and Vsx-2: two Chx10-like homeobox genes expressed in overlapping domains in the adult goldfish retina. J Comp Neurol 387:439–448.
Li L, Dowling JE (2000) Effects of dopamine depletion on visual sensitivity of zebrafish. J Neurosci 20:1893–1903.
Lillien L (1995) Changes in retinal cell fate induced by overexpression of EGF receptor. Nature 377:158–162.
Lima L, Urbina M, Matus P, Drujan Y (1996) Synthesis of serotonin from 5-hydroxytryptophan in the post-crush retina: inhibition of in vitro outgrowth by the intraocular administration of the precursor. Neurochem Res 21:939–946.
Link BA, Fadool JM, Malicki J, Dowling JE (2000) The zebrafish young mutation acts non-cell-autonomously to uncouple differentiation from specification for all retinal cells. Development 127:2177–2188.
Lyall AH (1957) Cone arrangements in teleosts retinas. Q J Microsc Sci 98:189–201.
Malicki J, Driever W (1999) oko meduzy mutations affect neuronal patterning in the zebrafish retina and reveal cell-cell interactions of the retinal neuroepithelial sheet. Development 126:1235–1246.
Marc RE, Sperling HG (1976) The chromatic organization of the goldfish cone mosaic. Vision Res 16:1211–1224.
McAvoy JW, Chamberlain CG (1990) Growth factors in the eye. Prog Growth Factor Res 2:29–43.
Moiseiwitsch JR (2000) The role of serotonin and neurotransmitters during craniofacial development. Crit Rev Oral Biol Med 11:230–239.
Mora-Ferrer C, Yazulla S, Studholme KM, Haak-Frendscho M (1999) Dopamine D1-receptor immunolocalization in goldfish retina. J Comp Neurol 411:705–714.
Negishi K, Teranishi T, Kato S (1982) New dopaminergic and indoleamine-accumulating cells in the growth zone of goldfish retinas after neurotoxic destruction. Science 216:747–749.
Negishi K, Teranishi T, Kato S (1985) Growth rate of a peripheral annulus defined by neurotoxic destruction in the goldfish retina. Brain Res 352:291–295.
Neophytou C, Vernallis AB, Smith A, Raff MC (1997) Muller-cell-derived leukaemia inhibitory factors arrests rod photoreceptor differentiation at a postmitotic pre-rod stage of development. Development 124:2345–2354.
Neumann CJ, Nuesslein-Volhard C (2000) Patterning of the zebrafish retina by a wave of sonic hedgehog activity. Science 289:2137–2139.
Paspalas CD, Goldman-Rakic PS (2004) Microdomains for dopamine volume neurotransmission in primate prefrontal cortex. J Neurosci 24:5292–5300.
Raven MA, Reese BE (2002) Horizontal cell density and mosaic regularity in pigmented and albino mouse retina. J Comp Neurol 454:168–176.
Raven MA, Eglen SJ, Ohab JJ, Reese BE (2003) Determinants of the exclusion zone in dopaminergic amacrine cell mosaics. J Comp Neurol 461:123–136.
Reese BE, Harvey AR, Tan S-S (1995) Radial and tangential dispersion patterns in the mouse retina are cell-class specific. Proc Natl Acad Sci USA 92:2494–2498.
Reese BE, Necessary BD, Tam PP, Faulkner-Jones B, Tan S-S (1999) Clonal expansion and cell dispersion in the developing mouse retina. Eur J Neurosci 11:2965–2978.
Reh TA, Tully T (1986) Regulation of tyrosine hydroxylase-containing amacrine cell number in larval frog retina. Dev Biol 114:463–469.
Rockhill RL, Euler T, Masland RH (2000) Spatial order within but not between types of retinal neurons. Proc Natl Acad Sci USA 97:2303–2307.
Rodieck RW (1991) The density recovery profile: a method for the analysis of points in the plane applicable to retinal studies. Vis Neurosci 6:95–111.
Rodrigues P, Dos S, Dowling JE (1990) Dopamine induces neurite retraction in retinal horizontal cells via diacylglycerol and protein kinase C. Proc Natl Acad Sci USA 87:9693–9697.
Scheer N, Groth A, Hans S, Campos-Ortega JA (2001) An instructive function for Notch in promoting gliogenesis in the zebrafish retina. Development 128:1099–1107.
Stenkamp DL, Frey RA, Prabhudesai SN, Raymond PA (2000) Function for hedgehog genes in zebrafish retinal development. Dev Biol 220:238–252.
Stenkamp DL, Powers MK, Carney LH, Cameron DA (2001) Evidence for two distinct mechanisms of neurogenesis and cellular pattern formation in regenerated goldfish retinas. J Comp Neurol 431:363–381.
Vaney DI (1994) Patterns of neuronal coupling in the retina. Prog Retin Eye Res 13:301–355.
Waid DK, McLoon SC (1998) Ganglion cells influence the fate of dividing retinal cells in culture. Development 125:1059–1066.

Wässle H, Boycott BB (1991) Functional architecture of the mammalian retina. Philos Trans R Soc Lond B Biol Sci 200:441–461.
Wässle H, Riemann HJ (1978) The mosaic of nerve cells in the mammalian retina. Physiol Rev 71:447–480.
Wässle H, Peichl L, Boycott BB (1983) Mosaics and territories of cat retinal ganglion cells. Prog Brain Res 58:183–190.
Watanabe T, Raff MC (1992) Diffusible rod-promoting signals in the developing rat retina. Development 114:899–906.
Watling KJ, Parkinson D, Dowling JE (1982) Effects of intraocular injections of 6-hydroxydopamine on dopamine-dependent cyclic AMP accumulation in intact pieces of carp retina. Brain Res 253:334–336.
Wikler KC, Rakic P (1990) Distribution of photoreceptor subtypes in the retinal of diurnal and nocturnal primates. J Neurosci 10:3390–3401.
Williams DR (1988) Topography of the foveal cone mosaic in the living human eye. Vision Res 28:433–454.
Yazulla S, Studholme KM (1997) Differential reinnervation of retinal bipolar cell dendrites and axon terminals by dopamine interplexiform cells following dopamine depletion with 6-OHDA. J Comp Neurol 382:535–545.
Yazulla S, Studholme KM (2001) Neurochemical anatomy of the zebrafish retina as determined by immunocytochemistry. J Neurocytol 30:551–592.
Yurco P, Cameron DA (2005) Responses of Müller glia to retinal injury in adult zebrafish. Vision Res 45:991–1002.
Zachor DA, Moore JF, Brezausek C, Theibert A, Percy AK (2000) Cocaine inhibits NGF-induced PC12 cells differentiation through D(1)-type dopamine receptors. Brain Res 869:85–97.